HHS Public Access

Author manuscript

Radiat Res. Author manuscript; available in PMC 2024 March 01.

Published in final edited form as:

Radiat Res. 2023 March 01; 199(3): 217–228. doi:10.1667/RADE-22-00048.1.

Characterization of the Response of 9L and U-251N Orthotopic Brain Tumors to 3D Conformal Radiation Therapy

O. Grahm Valadie[a,b,c], **Stephen L. Brown**[b,c,d,1], **Katelynn Farmer**[a], **Tavarekere N. Nagaraja**[e], **Glauber Cabral**[a], **Sheldon Shadaia**[a], **George W. Divine**[f], **Robert A. Knight**[a,g], **Ian Y. Lee**[e], **Jennifer Dolan**[b], **Sam Rusu**[a], **Michael C. Joiner**[c], **James R. Ewing**[a,d,e,g]

[a]Department of Neurology, Henry Ford Hospital, Detroit, Michigan

[b]Department of Radiation Oncology, Henry Ford Hospital, Detroit, Michigan

[c]Department of Radiation Oncology, Wayne State University, Detroit, Michigan

[d]Department of Radiology, Michigan State University College of Human Medicine, East Lansing, Michigan

[e]Department of Neurosurgery, Henry Ford Hospital, Detroit Michigan

[f]Department of Public Health Sciences, Henry Ford Hospital, Detroit Michigan

[g]Department of Physics, Oakland University, Rochester, Michigan

Abstract

In a study employing MRI-guided stereotactic radiotherapy (SRS) in two orthotopic rodent brain tumor models, the radiation dose yielding 50% survival (the TCD_{50}) was sought. Syngeneic 9L cells, or human U-251N cells, were implanted stereotactically in 136 Fischer 344 rats or 98 RNU athymic rats, respectively. At approximately 7 days after implantation for 9L, and 18 days for U-251N, rats were imaged with contrast-enhanced MRI (CE-MRI) and then irradiated using a Small Animal Radiation Research Platform (SARRP) operating at 220 kV and 13 mA with an effective energy of ~70 keV and dose rate of ~2.5 Gy per min. Radiation doses were delivered as single fractions. Cone-beam CT images were acquired before irradiation, and tumor volumes were defined using co-registered CE-MRI images. Treatment planning using MuriPlan software defined four non-coplanar arcs with an identical isocenter, subsequently accomplished by the SARRP. Thus, the treatment workflow emulated that of current clinical practice. The study endpoint was animal survival to 200 days. The TCD_{50} inferred from Kaplan-Meier survival estimation was approximately 25 Gy for 9L tumors and below 20 Gy, but within the 95% confidence interval in U-251N tumors. Cox proportional-hazards modeling did not suggest an effect of sex, with the caveat of wide confidence intervals. Having identified the radiation dose at which approximately half of a group of animals was cured, the biological parameters that accompany radiation response can be examined.

[1]Correspondence to: Stephen Brown, PhD, Director of Radiation Biology Research, Radiation Oncology, Henry Ford Health System, 2799 West Grand Blvd, Detroit, MI 48202-2689; sbrown1@hfhs.org.

INTRODUCTION

Despite the aggressive therapies available to patients with a grade IV astrocytoma (known as a glioblastoma multiforme or GBM), the mean life expectancy from diagnosis to death remains at around 15 months (1, 2). However, about 5% of treated patients survive to the five-year mark. The current standard treatment involves maximally safe surgical resection followed by radiation therapy over a 6-week period with concomitant temozolomide (TMZ) chemotherapy, followed by TMZ maintenance (3). The underlying, and potentially life-preserving, biology associated with these patients' response to cytotoxic therapy is not yet well understood. Further exploration into the measures that differentiate survivors from non-survivors could be a key to directing therapy.

Discriminants that differentiate survivors from non-survivors have been observed in small animal models. For instance, acute (hours) vascular changes after a single 20 Gy dose of radiation in small animal models of cerebral tumors have been observed (4). This presents the question of whether measured physiological changes might be used to predict a curative response in animal models, and thereby inform future clinical choices. A sampling strategy that produces a roughly equal proportion of cures and failures is thus important for two reasons. First, to understand the physiology that contributes to radiation response. Second, to potentially construct a predictor of radiation response based on noninvasive measures of tumor physiology.

Accordingly, an MRI-based study (NIH/NCI R01-CA218596) was initiated to measure acute changes in tumor physiology as predictors of survival. While the COVID-19 pandemic interrupted aspects of this study, enough information was available for an estimate of the tumor control dose in half of the animals treated (the TCD_{50}). The purpose of this study is the determination of the radiation dose for survival in a design that utilizes contrast-enhanced MRI (CE-MRI) for conformally targeted treatment of two commonly used orthotopic tumor models. While this study is preliminary to a larger study of the physiology of response in small-animal models of stereotactic radiosurgery (SRS), it should be useful as a benchmark study in other preclinical investigations (e.g., approaches that employ adjuvants to radiotherapy).

Conformal radiotherapy displays superior dose distributions when compared to single beam therapies in both small animal models and their human counterparts (5–7). The Small Animal Radiation Research Platform (SARRP) (Xstrahl Medical and Life Sciences, Suwanee, GA) is a change of delivery method from a single or parallel-opposed stationary radiation beam(s) delivered by a standard linear accelerator in other preclinical studies (4, 8, 9). While there are differences from clinical linear accelerators in beam quality, the SARRP presents an example of new instrumentation allowing rodent subjects to be treated more like their human counterparts in terms of set-up (immobilization, pre-irradiation cone beam computer tomography (CBCT)), treatment planning (treating based on co-registered CBCT/MRI images), and treatment delivery (conformal therapy).

As methods in small animal conformal therapy evolve, there is a call for the establishment of relevant dosimetric standards (10–13). Because the technology now allows for more

precise clinically relevant therapies in small animal models, baseline studies are needed to establish important radiological landmarks for rodent models. Of the available landmarks, because it is a measure of response in the entire population of cells in the tumor, “the most relevant measure of tumor response is TCD_{50}” (14). In this study, two widely employed tumor models of GBM, U-251N in athymic rats, and 9L in Fischer rats, were studied in roughly equal numbers of male and female animals. Radiation doses were adjusted to yield approximately equal numbers of complete response and failure in the two models. To our knowledge, because it utilizes conformal radiation in small-animal models of cerebral tumors, this work presents a unique data set of long-term survival after conformal, high-dose irradiation for the two tumor models studied.

In addition to identifying a TCD_{50}, the effects of tumor volume at the time of treatment and biological sex on survival were also assessed. Both factors are vital components of a comprehensive tumor model study and therefore continue to be areas of interest in clinical research.

While small-animal studies in response to radiotherapy may be limited in their ability to precisely match therapeutic prescriptions in humans, they have value. These models allow for a uniform sample of subjects to be treated with a range of therapies, exposed to alternate and adjuvant therapies, and examined in depth post-treatment, activities that are not possible in clinical studies. This study addresses the problem of determining a radiation dose that yields examples of both success and failure in an animal model with roughly equal likelihood. As such this study presents an important first step in determining if biological factors are associated with response to high dose radiation in these animal models of GBM.

MATERIALS AND METHODS

Animals and Tumor Cells

All animal studies were done under an Institutional Animal Care and Use Committee (IACUC)-approved protocol (#1604). This work studied an approximately equal number of male and female 136 Fischer 344 rats (10–12 weeks old and 200–230 g), and 98 RNU athymic rats (10–12 weeks old and 200–230 g) (Charles River Laboratories, Wilmington, MA), implanted with rat 9L and human U-251N cells, respectively. 9L and U-251N cells were maintained in Dulbecco’s Minimum Essential Media (DMEM) with 10% fetal bovine serum (FBS) and 1% streptomycin and penicillin. Cell cultures were passaged once a week and not more than 4 times. Approximately once a month, frozen stock from an early passage of the original cells (9L from ATCC, Manassas, VA and U-251N from Dr. T. Mikkelsen, Henry Ford Health System, Detroit, MI) were thawed and used. Logphase growth cells were harvested for implantation (see below for implantation details). The concentrations of rat 9L and human U-251N cells were 2×10^8 cells per mL and 5×10^9 cells per mL, respectively, which were loaded into a 10 μL Hamilton syringe (Model 701, Hamilton Co., Reno, NV) before implantation.

Implantation

Cell implantation followed methods published previously (15, 16). Animals were anesthetized with isoflurane (3% for induction, 1–2% for maintenance, balance N_2O:O_2 = 2:1). A 1-cm incision was made 2 mm to the right of the midline and the skull was exposed. A burr hole was drilled 3.5 mm to the right of the bregma, taking care not to penetrate the dura mater. A 10 μL Hamilton syringe with a 26-gauge needle containing 2×10^4 9L (n = 136) or 5×10^5 U-251N (n = 98) tumor cells in 10 μl of phosphate buffered saline (Life Technologies, Carlsbad, CA), was lowered to a depth of 3.0 mm and then raised back to a depth of 2.5 mm to create a pocket. Cancer cells were injected at a rate of 0.5 μL/10 s.

MRI

All studies used a Varian/Magnex (Santa Clara, CA), 7 Tesla, 20 cm bore magnet with a Bruker console running Paravision 6.0 software. Gradient maximum strengths and rise times were 250 mT/m and 120 μs. Following published procedures (4, 16, 17), all two-dimensional MRI image sets were acquired with a 32×32 mm^2 field of view (FOV). Transmit and receive coils included a Bruker Quadrature Birdcage (transmit) and 4-channel phased-array surface coil receiver (Rapid MR International, Columbus, OH). T1-weighted images (T1WIs) were acquired pre- and post-tail-vein administration of the contrast agent (Magnevist©, Bayer Healthcare Pharmaceuticals, Wayne, NJ, 0.25 mmol/kg) with the following parameters: matrix: 256 × 192 pixels, 27 slices, 0.4 mm thickness, 0.1 mm gap, number of echoes (NE) = 1, number of averages (NA) = 4, TE/TR = 16/800 ms. To co-register the MRI with CBCT images, an additional FLASH three-dimensional gradient-echo sequence was employed post-contrast with the following parameters: matrix size 256 × 192x96 voxels, 1 slice, slice thickness 24 mm, echo time 2.7 s, FOV, $42 \times 32 \times 24$ mm^3, spatial resolution of $0.164 \times 0.167 \times 0.25$ mm^3, number of echoes (NE) = 1, number of averages (NA) = 1, tip angle 20°.

CT and Treatment

Treatment timeline is outlined in Fig. 1. Animals of either sex were randomly assigned as untreated controls or irradiated in a ratio of approximately 1:2 (controls:treated); numbers are summarized in Table 1. The dose of radiation was chosen with the goal that the radiation exposure would be curative (i.e., animals would survive 200 days) in approximately half of the group of animals.

Tumor readiness for treatment was assessed on the largest, post-contrast, coronal slice of the tumor during a size check; if the distance from top to bottom of the embedded portion of the tumor was at least 3–4 mm, the tumor was deemed large enough for treatment. Animals were irradiated using a SARRP arranged as in Fig. 2. The SARRP operated at 220 kVp and 13 mA. With the 0.15-mm beam-hardening copper filter, the effective energy was approximately 70 keV. Under isoflurane anesthesia (3% for induction, 1–2% for maintenance, balance N_2O:O_2 = 2:1), rats were imaged by the SARRP's CBCT and irradiated in a temperature-controlled cradle with heads held in place by bite piece. Orientation was assessed using CBCT and tumor location was co-registered to 3D-GRE images. Treatment planning using Xstrahl's MuriPlan software was used to deliver four non-coplanar arcs with an identical isocenter located at the approximate center of the tumor

volume. Tumors were treated to 80% isodose. The resultant dose rate was approximately 2.5 Gy per min.

Radiation Dose Quality and Delivery Assurance

Preliminary studies suggested that the TCD_{50} was in the vicinity of 20 Gy (4, 9). As the study progressed, it became apparent that 20 Gy was yielding low survival for the 9L animals, and this value was increased to 25 Gy.

The dose calculation accuracy of MuriPlan was validated for the SARRP. Radiation measurements were made using a small-sized cylindrical ion chamber (PTW PinPoint Ion Chamber Type 31014, Freiburg, Germany), 2 mm in diameter with a sensitive volume of 0.015 cm^3. The ion chamber was positioned in a water tank in the center of a 10 × 10 mm collimated beam. Radiation dose was measured as a function of depth from the water surface. The half-value thickness of water for 220 kVp photons is approximately 25 cm assuming an effective energy of 70 keV (18). The radiation beam quality was characterized using the tube potential and half-value thickness following the guidelines of the American Association of Physicists in Medicine (AAPM) protocol for 40–300 kV X-ray beam dosimetry, Task Group-61 (19). Good agreement (2.0 ± 3.0%) was found between the measured physical dose and the MuriPlan dose calculation.

Radiation delivery was confirmed for each animal by the exposure of a small (approximately 5 cm^2) piece of EBT3 Gafchromic film (Ashland, Bridgewater, NJ) that was placed on the animal's head.

Endpoint - Survival

Rats were monitored daily after irradiation for weight loss and behavioral changes. The study endpoint was either death or symptom-free survival to 200 days postirradiation. When symptoms associated with tumor burden (inactivity, lethargy, hunching, porphyrin exudate, abnormal gait, and/or weight loss ≥20%) were observed, rats were euthanized by transcardial perfusion under 5% isoflurane anesthesia followed by decapitation, with the duration of survival recorded. Asymptomatic rats were euthanized in the same manner once the 200-day endpoint was reached.

Histology

After sacrifice, rat brains were removed and placed in a 4% paraformaldehyde solution for tissue fixation and stored in the same fixative at 4°C. They were cut using a rat brain matrix into 2-mm thick coronal slices and embedded in paraffin. Slices containing tumor tissue were then cut into 6-μm thick sections and placed on coated slides from Thermo Fisher Scientific (Waltham, MA) for staining. The presence and extent of the tumor were determined by light microscopy using hematoxylin and eosin (H&E) stained sections (15, 20, 21). In addition, immunostaining with human major histocompatibility complex (MHC) was used to identify U-251N cells, which are of human origin.

Image Processing for Volume Determination

The image analysis program Eigentool (Henry Ford Health Sciences, Department of Radiology, Detroit, MI) was used to confirm the alignment of the pre- and post-contrast T1-weighted MRI images, after which a subtraction process was performed (22, 23). The region of interest (ROI) tool in Eigentool was then used on every image in which tumor was visible in the resultant subtraction images to determine the number of contrasting voxels following established methods (24–26). This value was then translated to a corresponding volume.

An assumption of 0 mm^3 at time of implantation was made after multiple scans performed immediately after sham implantations failed to show any enhancing voxels in four animals of each strain. The lack of contrast at time of implantation implied that the surgery itself did not cause any physical phenomena that led to a signal, and it can therefore be assumed that scans immediately after implantation (t = 0 days) would show no indications of a tumor for all subjects.

Data Analysis

All statistical analyses were conducted using the R statistical packages (27). Using its survival analysis package (28), Kaplan-Meier survival curves were used to estimate the TCD_{50} dose and the proportion of animals alive and asymptomatic at the 200 day study endpoint. Groups of interest were separated by tumor type and treatment dose as presented in Table 1.

The effect of sex and tumor volume at time of treatment on survival was studied in sub-analyses. Kaplan-Meier estimation was re-done for each treatment group, this time additionally broken down by sex. A Cox Proportional-Hazards (Cox PH) model was used to estimate the hazard ratio (HR) associated with gender (male:female) at the 95% confidence interval (CI). For the test conducted in this study, a hazard ratio of 1.0 would imply that there was no effect of sex on survival while a HR of 0.5 would indicate females were twice as likely to die as females, etc.

R plotting routines were used to graph tumor volume at the time of treatment versus survival. A Wilcoxon Rank Sum/Mann-Whitney U test was performed to assess the relationship between tumor volume at time of treatment against survival as a binary outcome (0 = no death/sacrifice before 200 days, 1 = death before 200 days).

Growth curves were formed from volume estimates during untreated growth using subtraction images formed by pairs of pre- and post-contrast MRI images (both controls and tumors that would go on to be treated). To establish the initial model, each untreated growth measurement for which multiple pre-treatment studies existed (n_{9L} = 29, $n_{U\text{-}251N}$ = 39) was included and weighted as an independent measurement.

RESULTS

For survival studies, the final count was 61 male and 55 female for a total of 116 Fischer 344 rats and 35 male and 31 female for a total of 66 RNU athymic rats (see Table 1 for details of number and sex of treated and untreated rats).

Survival to the 200 day mark post-implantation appeared to be a reasonable benchmark after irradiation. Figure 3 shows histological slides and corresponding T_1-weighted post-contrast MRI images in untreated rats. The good correspondence between histology and MRI is consistent with previous studies (29). Conversely, no detectable tumor burden can be seen in sampled images of rats that survived to 200 days (Fig. 3). In a random sample (5 from each tumor type), ten animals that survived to 200 days were checked for residual tumor growth via pre-sacrifice MRI and post-sacrifice histology. No evidence of residual tumors was found.

Radiation Tumor Control Dose of 50%, Long-Term Survival

Kaplan-Meier survival analysis for rats treated with varying doses was used to first identify if a 50% survival had been achieved at 200 days. The results described in the following section are summarized in Table 2 and displayed visually in Fig. 4, with fractional survival (number of rats who lived to 200 days divided by total number of rats studied) plotted versus time post-tumor-implantation in days.

For rats implanted with 9L tumors, 25 Gy achieved 47.5% survival at 200 days, a marked improvement in survival compared to untreated or treated with 20 Gy. Figure 4A shows a survival comparison for control subjects (n = 30, red) versus those treated with 20 Gy (n = 22, black). Although the median survival increased from 9 days to 27 days, fractional survival for the 9L rats treated with 20 Gy still dropped to 0.227 ± 0.089 by 65 days and remained steady until the 200-day endpoint. Conversely, those animals treated with 25 Gy (Fig. 4B) had a median survival of 119 days with fractional survival at the 200-day endpoint being 0.475 ± 0.064. Figure 4B additionally shows that the 95% CI for the 25 Gy treated 9L animals falls centrally around the 50% survival goal. Assuming a locally linear relationship between survival and dose, these two points were used to estimate TCD_{50} for 9L tumors treated with conformal SRS to be approximately 25.5 Gy.

For rats implanted with U-251N tumors, more than half the animals treated with 20 Gy survived to 200 days, as seen in Fig. 4C. Compared to untreated controls where all animals died by 43 days, those treated with 20 Gy had a fractional survival of 0.628 ± 0.074 at the study endpoint. For the group treated at 20 Gy, the upper bound of the 95% CI fell above the goal of 50% survival and median survival fell above the 200 days as reported in Table 2. Thus, the 63% fractional survivals for U-251N tumors treated with conformal SRS therapy was achieved with 20 Gy as per this study.

One marked visual comparison between Fig. 4B and C was the consistency of the survival curve past the initial 60 days of survival. For the treated 9L group (Fig. 4B, black), survival dropped in the first two months after irradiation and then was maintained, apart from two

deaths, until the study endpoint. Comparatively, in the treated U-251N group (Fig. 4C, black), survival decreased with no marked pattern throughout the long-term study.

In 2020, the COVID-19 pandemic mandated the closure of our laboratory and forced the sacrifice of all animals in the survival study. For the survival analysis, these animals were censored, but still used for Kaplan-Meier estimation. The censored animals were removed from analyses for volume and sex effects on survival.

Potential Influences on Survival: Gender of Rats or Size of Tumor at Time of Irradiation

As noted, animals ($n_{9L} = 11$, $n_{U\text{-}251N} = 0$) were removed from future statistical tests due to COVID-19 shut down procedures. These animals were then excluded from size analyses vs. survival. Outliers ($n_{9L} = 3$, $n_{U\text{-}251N} = 1$) were excluded from the size analysis based on their lying outside the 95% interval in a box plot examination. Animals with no volume measurement within 24 h of treatment ($n_{9L} = 9$, $n_{U\text{-}251N} = 10$) were not included.

Kaplan-Meier survival estimates at each dose level were broken down by gender (Fig. 5) and were supplemented with a Cox PH analysis to evaluate the effect of gender on survival. The Cox PH model is a standard for investigating the association between survival and one or more predictor variables such as gender. The results of this analysis (Table 3) demonstrate that there are no statistically significant gender-related differences in response to radiation at any treatment dose used in this study. That being said, the two groups that had the highest suggestion of a difference were the 9L untreated controls [HR(M/F) = 1.88] and the U-251N 20 Gy [HR (M/F) = 0.51] groups. Conversely, the 20 Gy 9L group and U-251N untreated control group showed less extreme deviation between genders, while the 25 Gy 9L group had a HR of 1.06, indicating no difference between the two groups. The analysis of the study data suggests that there is no evidence for a difference in survival, although 95% confidence intervals are wide for all groups evaluated in this study.

The effect of tumor volume at the time of treatment on long-term survival was analyzed in both tumor models for those animals who received the ~TCD_{50} (25 Gy for 9L and 20 Gy for U-251N models). A summary of volume at time of treatment statistics for survivors and non-survivors (Table 4) displays differences between the two tumor cell lines. For the U-251N animals, the survivors had both a higher mean volume and a wider range of tumors. The opposite was true for the 9L group. These trends (Table 4), discussed below, were further evaluated by plotting volume data at time of treatment against survival post-implantation (Fig. 6).

Although typical tumors presented with a largest dimension of 3–4 mm in the coronal plane, their volumes varied widely; tumor volumes for the ~TCD_{50} groups were ~20–550 mm^3 for U-251N tumors and ~10–300 mm^3 for 9L tumors. Figure 6A (9L tumors) depicts that, aside from one animal, all rats with tumor volumes above the average tumor volume at time of treatment did not survive to the study endpoint. Conversely, a Wilcoxon Rank-Sum test run on the same data resulted in a P value of 0.159 suggesting that there was no statistically significant difference between survivors and non-survivors. This remains true when the animals were divided by sex; the results again do not support a significant difference in tumor sizes between survivors and non-survivors (Table 5).

There is no statistical correlation between tumor size at time of treatment and survival for the U-251N group (P = 0.223) within the volume range. This finding persists when each sex is tested individually. Additionally, there is no apparent difference between tumor sizes for those animals that died between 60- and 200 days post-implantation. The continuous falloff in survival to the 200-day endpoint is a distinguishing characteristic of the U-251N survival curve. There is no notable sex or tumor volume influence in this interval of time, as shown in Fig. 6B.

Overall, these data suggest no significant correlation between the measured tumor volume and survival in the animals assessed in this study. Additionally, this result does not change if the sexes are evaluated separately.

Growth Curves of Untreated Tumors

Measurements of volume were available around the time of irradiation as follows 1. volumes measured the day before but within 24 h of treatment, 2. volumes measured the day of and before treatment, 3. volumes measured the day of and within 6 h after treatment. These groups were tested for differences in the mean volume. Groups 1 and 3 were both individually compared with group 2 using a two-sided t-test. Neither group 1 nor group 3 varied significantly from group 2. Therefore, data from all three groups were used. In the rare case (n = 2) that multiple volume data from the same animal were available, the data collected closest in time to the treatment was used.

Growth plots (Fig. 7) show that 9L tumors achieved 3 to 5 mm largest dimension in the coronal plane in approximately 7 days, i.e., a large enough size to be treated, while U-251N tumors needed 18 days to achieve a similar size. Figure 7A shows growth for 9L tumors from 2 to 14 days post-implantation The majority of data collected was taken between 6–9 days post-implantation. After little change for the first 6 days of growth, the mean tumor value rises as an approximate exponential until 10 days post-implantation. After this point, with removal of animals for study, no trend should be inferred.

Figure 7B shows the same data for untreated U-251N tumors over an interval of 40 days. Up until to 25 days, the mean volume increases slowly; plateauing for a few days before rising again. Again, after this point, with removal of animals for irradiation, no trend should be inferred.

Data presented in Figs. 3–6 are located at a web-accessible repository; access is available upon request to James R. Ewing, jewing1@hfhs.org.

DISCUSSION

This paper has presented an estimate of the TCD_{50} using a single fraction radiation dose in two models of cerebral tumor. The doses that resulted in complete response in 50% of each tumor population dose were near, but less than 20 Gy for U-251N and about 25 Gy for 9L tumors. In the 9L tumor population, even suboptimal doses increased survival expectations. Tumor size and sex demonstrated no significant effects when considered as cofactors of radiation response, given the sample sizes. These measures of radiation response can supply

a benchmark to other investigators using conformal irradiation. Looking forward, they form the basis of a process intended to form a predictor of survival based on measures of cerebral physiology.

MRI, universally employed for standard radiation treatment planning, also offers the possibility of establishing novel strategies for patient-specific treatment planning for high-grade brain tumors (30). Thus, preclinical models need to be comprehensive in their reporting of potential contributors, e.g., tumor volume, sex, to survival and treatment response (21, 30, 31). Tumor volume of both primary and secondary brain tumors has been tied to radiation treatment success. Larger tumor volumes require higher dose regimes and lower volumes have been correlated to treatment success (9, 32). The support for biological sex contributing to treatment response is mixed. A long-term comparison of patient data treated both before and after the introduction of the current standard of care has shown no statistically significant difference between sexes (33), while other reports suggested women have a better prognosis than men for primary GBM cases (34–36). Much work is needed to confirm gender effects in high-grade glioma cases, and the potential contribution of sex-specific treatment plans (35).

Post-surgical irradiation is part of the standard of care for both primary and recurring high-grade gliomas. As the treatment of glioblastoma has advanced to include high-dose radiation, reliable pre-clinical models should similarly be advanced. To meet that need, this study aimed to utilize technology that allowed for the implementation of high-dose conformal therapy with normal tissue sparing to achieve a curative dose in a fraction of the treated population.

This study employed a high-dose, single fraction treatment; in that it differed from the standard of care for GBMs and other high-grade gliomas. This allows the quantification of the simplest possible dose regime so that the value can then be used to calculate potential TCD_{50}'s for a variety of other dose regimes. While the radiation arm of the clinical standard of care for high-grade gliomas 54–60 Gy in 6–8 fractioned doses delivered 2–3 times a week for six weeks, a variety of dose prescriptions are under study (37). The standard of care is based on temporal fractionation to allow for tumor reoxygenation, cell cycle redistribution, and reduced normal tissue toxicity. In the past ten years the potential benefits of hypofractionation or single fractionated SRS on high-grade gliomas (38–40) have been investigated in multi-institutional trials. For instance, studies included dose prescription for GBM treatment that ranged from 40 Gy in sixteen fractions to 20 Gy in 5 fractions (38). Because many fractionation schemes are still being explored, the experimental design started at the simplest case that might be used as a baseline for a variety of other treatment plans.

This study was limited in its precision: survival at 20 Gy was barely within the 95% confidence interval for the goal of 50% tumor control for U-251N animals treated. For 9L tumors treated at 25 Gy, a better estimate resulted. The necessity of retaining animals for up to 200 days made it difficult to know with great precision if the given dose was correct, particularly when the dose cured at a higher rate than intended. For the 9L animals, it was soon evident that 20 Gy was below a curative dose for 50% of the population. For the U-251N group, however, 20 Gy achieved a control higher than 50%. For future use, and for

the benefit of other investigators, we note that approaching the TCD_{50} dose from below is much more efficient in time than starting from above.

Because subsequent research was designed to identify MRI biomarkers of survival, these data are usable, since they are adequately populated by survivors and non-survivors. Ideally, future research will adjust dosages to better estimate TCD_{50}'s in these models.

When considering potential reasons for the different TCD_{50} for each cell line, retrospective in vitro data from a common lab where plated cells were treated with radiation alone in known doses as control studies were used to calculate common radiobiological benchmarks [α/β, biological effective dose (BED), and equivalent dose in 2 Gy fractions (EQD_2)] from a linear-quadratic fit to the resulting survival data. When fit to a linear-quadratic trend line, retrospective U251N data (41) gave an α/β value of 9.1 Gy. From this value, A BED value of 64.0 Gy, and an EQD_2 value of 52.4 Gy can be calculated for a reference dose of 20 Gy in a single fraction. Likewise, references several in vitro 9L survival studies (42, 43), the average α/β value was 9.0 Gy, yielding a BED of 94.4 Gy and EQD_2 of 59.1 Gy for a reference dose of 25 Gy in a single fraction. The calculated α/β values for each cell line are similarly based on the retrospective in vitro data; this potentially indicates that the reasons for the varying responses can only be determined by future examination of in vivo conditions.

While tumor size and sex were not determined to influence response, this study has limited power to consider subgroup analyses. These findings should be taken with some caution. In the case of tumor size and response to radiation not demonstrating a significant relationship, this is of particular importance. Contrary to our findings, previous studies in 9L tumors have shown that larger tumors require higher radiation doses to be treated effectively (44). However, the present study differs in the radiation delivery from those studies because of the use of conformal radiation. Additionally, the tumors treated in this study were limited to those with a largest dimension of 3–5 mm. While that dimension resulted in a wide range of volumes, the range of tumor sizes was still limited. Further investigation would be needed to determine how the method of radiation delivery and the limited tumor size range influences these results.

This study supports the suggestion that biological sex does not contribute to radiation response (33). If supported by future study, this could be of interest to the preclinical community. Currently National Institutes of Health (NIH) requires all animal studies to include equal numbers of male and female animals unless there is a strong justification for single-sex studies (45). Should sex continue to have null-effects in preclinical GBM models of radiation response, an argument might be made to limit it to one gender, thus greatly reducing the resources required for an animal study and allowing for larger study impacts.

Bias due to sample removal along the timeline may be introduced in the growth plots because treated animals, as opposed to untreated controls, were removed from the study when the tumor volume was large enough for treatment. Thus, these curves are best utilized for establishing a treatment window for each cell line based on in vivo growth. For example, if a study wanted to treat/test animals immediately before rapid growth occurs in vivo, a

treatment window of 7–9 days for 9L and 17–18 days for U-251N can be seen in the growth plots.

Rapidly growing tumors of all types, including high-grade astrocytomas (Grade 3 or 4), typically exhibit blood-brain barrier (BBB) breakdown as a radiological sign. Folkman has demonstrated that tumor growth beyond a diameter of ~300 microns is metabolically dependent on angiogenesis, which is accompanied in the brain by BBB breakdown (46–48). Low-grade (1 or 2), slower-growing astrocytomas do not typically exhibit BBB breakdown. In our case, our inplane resolution was 150 μm, and the limit of detection was 2 and 4 mm^3 for U-251N and 9L tumors, respectively.

The volumes of U-251N tumors are markedly larger when compared to that of 9L tumors. Due to the typically leaky nature of both tumor models, the contrast is carried by tumor exudate into the surrounding tissue, causing a “halo” which is not easily distinguished from the tumor volume in the subtraction image (17, 49). It is our impression that 9L tumors do not typically have as large a halo as U-251N tumors; the possible differential effect of this halo was not accounted for in the reported volumes presenting a potential bias in the volume estimates.

COVID-19 shutdown protocols affected our collection of long-term survival data. Animals being evaluated for long-term survival were sacrificed early due to national mandates. Such animals could be included in Kaplan-Meier survival curves, but both data and power to make stronger conclusions were lost.

This work determined radiation doses that can generate approximately equal number of survivors and non-survivors to be studied; a first step in evaluating biological factors as early predictors of response to radiation and long-term survival utilizing the non-invasive technique of CE-MRI. Growth plots and radiation response of orthotopic 9L and U-251N tumors were characterized in rodent models in terms of a clinically relevant treatment technique. The effect of growth and sex were studied in these models, without finding a significant effect. The radiation dose that cures half of a group of animals with tumors was estimated. The influence of tumor volume at time of treatment as measured using CE-MRI T1 subtraction images was evaluated. Future studies will examine what set of pre-treatment MRI biomarkers (e.g., blood flow, vascular permeability, etc.) predicts response in these models.

ACKNOWLEDGEMENTS

The authors thank Jun Xu for her excellent technical assistance. Research reported in this publication was also supported by the National Cancer Institute of the National Institutes of Health under award number R01-CA218596 (Ewing/Brown).

REFERENCES

1. Johnson DR, O’Neill BP. Glioblastoma survival in the United States before and during the temozolomide era. J Neurooncol 2012; 107(2):359–64. [PubMed: 22045118]
2. Patel MA, Kim JE, Ruzevick J, Li G, Lim M. The future of glioblastoma therapy: synergism of standard of care and immunotherapy. Cancers (Basel) 2014; 6(4):1953–85. [PubMed: 25268164]

3. Oronsky B, Reid TR, Oronsky A, Sandhu N, Knox SJ. A Review of Newly Diagnosed Glioblastoma. Front Oncol 2020; 10:574012. [PubMed: 33614476]
4. Brown SL, Nagaraja TN, Aryal MP, Panda S, Cabral G, Keenan KA, et al. MRI-Tracked Tumor Vascular Changes in the Hours after Single-Fraction Irradiation. Radiat Res 2015; 183(6):713–21. [PubMed: 26010711]
5. Bazalova M, Nelson G, Noll JM, Graves EE. Modality comparison for small animal radiotherapy: a simulation study. Med Phys 2014; 41(1):011710. [PubMed: 24387502]
6. Bolcaen J, Descamps B, Boterberg T, Vanhove C, Goethals I. PET and MRI Guided Irradiation of a Glioblastoma Rat Model Using a Micro-irradiator. J Vis Exp 2017(130).
7. Thibouw D, Truc G, Bertaut A, Chevalier C, Aubignac L, Mirjolet C. Clinical and dosimetric study of radiotherapy for glioblastoma: three-dimensional conformal radiotherapy versus intensity-modulated radiotherapy. J Neurooncol 2018; 137(2):429–38. [PubMed: 29374810]
8. Mowday AM, Lieuwes NG, Biemans R, Marcus D, Rezaeifar B, Reniers B, et al. Use of a Luciferase-Expressing Orthotopic Rat Brain Tumor Model to Optimize a Targeted Irradiation Strategy for Efficacy Testing with Temozolomide. Cancers (Basel) 2020; 12(6).
9. Kim JH, Khil MS, Kolozsvary A, Gutierrez JA, Brown SL. Fractionated radiosurgery for 9L gliosarcoma in the rat brain. Int J Radiat Oncol Biol Phys 1999; 45(4):1035–40. [PubMed: 10571213]
10. Biglin ER, Price GJ, Chadwick AL, Aitkenhead AH, Williams KJ, Kirkby KJ. Preclinical dosimetry: exploring the use of small animal phantoms. Radiat Oncol 2019; 14(1):134. [PubMed: 31366364]
11. Bolcaen J, Descamps B, Deblaere K, Boterberg T, Hallaert G, Van den Broecke C, et al. MRI-guided 3D conformal arc micro-irradiation of a F98 glioblastoma rat model using the Small Animal Radiation Research Platform (SARRP). J Neurooncol 2014; 120(2):257–66. [PubMed: 25069566]
12. Dos Santos M, Kereselidze D, Gloaguen C, Benadjaoud MA, Tack K, Lestaevel P, et al. Development of whole brain versus targeted dentate gyrus irradiation model to explain low to moderate doses of exposure effects in mice. Sci Rep 2018; 8(1):17262. [PubMed: 30467388]
13. Rutherford A, Stevenson K, Tulk A, Chalmers AJ. Evaluation of four different small animal radiation plans on tumour and normal tissue dosimetry in a glioblastoma mouse model. Br J Radiol 2019; 92(1095):20180469. [PubMed: 30362815]
14. Hall EJ. Radiobiology for the radiologist Hagerstown, MD: Medical Dept.; 1973. xi, 305 p.
15. Elmghirbi R, Nagaraja TN, Brown SL, Panda S, Aryal MP, Keenan KA, et al. Acute Temporal Changes of MRI-Tracked Tumor Vascular Parameters after Combined Anti-angiogenic and Radiation Treatments in a Rat Glioma Model: Identifying Signatures of Synergism. Radiat Res 2017; 187(1):79–88. [PubMed: 28001908]
16. Elmghirbi R, Nagaraja TN, Brown SL, Keenan KA, Panda S, Cabral G, et al. Toward a noninvasive estimate of interstitial fluid pressure by dynamic contrast-enhanced MRI in a rat model of cerebral tumor. Magn Reson Med 2018; 80(5):2040–52. [PubMed: 29524243]
17. Ewing JR, Bagher-Ebadian H. Model selection in measures of vascular parameters using dynamic contrast-enhanced MRI: experimental and clinical applications. NMR Biomed 2013; 26(8):1028–41. [PubMed: 23881857]
18. Johns HE, Cunningham JR. The physics of radiology 4th ed. Springfield, Ill., U.S.A.: Charles C. Thomas; 1983. xix, 796 pages p.
19. Ma CM, Coffey CW, DeWerd LA, Liu C, Nath R, Seltzer SM, et al. AAPM protocol for 40–300 kV x-ray beam dosimetry in radiotherapy and radiobiology. Med Phys 2001; 28(6):868–93. [PubMed: 11439485]
20. Nagaraja TN, deCarvalho AC, Brown SL, Griffith B, Farmer K, Irtenkauf S, et al. The impact of initial tumor microenvironment on imaging phenotype. Cancer Treat Res Commun 2021; 27:100315. [PubMed: 33571801]
21. Nagaraja TN, Aryal MP, Brown SL, Bagher-Ebadian H, Mikkelsen T, Yang JJ, et al. Cilengitide-induced temporal variations in transvascular transfer parameters of tumor vasculature in a rat glioma model: identifying potential MRI biomarkers of acute effects. PLoS One 2013; 8(12):e84493. [PubMed: 24376814]

22. Peck DJ, Windham JP, Emery LL, Soltanian-Zadeh H, Hearshen DO, Mikkelsen T. Cerebral tumor volume calculations using planimetric and eigenimage analysis. Med Phys 1996; 23(12):2035–42. [PubMed: 8994168]
23. Peck DJ, Spickler EM, Knight RA, Hearshen DO, Windham JP. Analysis of the evolution of focal cerebral ischemia in the rat using the eigenimage filter. Magn Reson Med 1992; 26(2):259–73. [PubMed: 1513250]
24. Gelman N, Ewing JR, Gorell JM, Spickler EM, Solomon EG. Interregional variation of longitudinal relaxation rates in human brain at 3.0 T: relation to estimated iron and water contents. Magn Reson Med 2001; 45(1):71–9. [PubMed: 11146488]
25. Bagher-Ebadian H, Nagaraja TN, Paudyal R, Whitton P, Panda S, Fenstermacher JD, et al. MRI estimation of contrast agent concentration in tissue using a neural network approach. Magn Reson Med 2007; 58(2):290–7. [PubMed: 17654573]
26. Bagher-Ebadian H, Jafari-Khouzani K, Mitsias PD, Lu M, Soltanian-Zadeh H, Chopp M, et al. Predicting final extent of ischemic infarction using artificial neural network analysis of multi-parametric MRI in patients with stroke. PLoS One 2011; 6(8):e22626. [PubMed: 21853039]
27. Team RC. R: A language and environemnt for statistical computering R Foundation for Statistical Computing, Viennta, Austria2020.
28. Therneau TM. A Package for Survival Analysis in R. Release 3.2–13 https://libraries.io/cran/survival/3.2-13.
29. Vullo T, Deo-Narine V, Stallmeyer MJ, Gomez DG, Cahill PT. Quantitation of normal canine hippocampus formation volume: correlation of MRI with gross histology. Magn Reson Imaging 1996; 14(6):657–62. [PubMed: 8897370]
30. Connor M, Kim MM, Cao Y, Hattangadi-Gluth J. Precision Radiotherapy for Gliomas: Implementing Novel Imaging Biomarkers to Improve Outcomes With Patient-Specific Therapy. Cancer J 2021; 27(5):353–63. [PubMed: 34570449]
31. Swinburne N, LoCastro E, Paudyal R, Oh JH, Taunk NK, Shah A, et al. Computational Modeling of Interstitial Fluid Pressure and Velocity in Non-small Cell Lung Cancer Brain Metastases Treated With Stereotactic Radiosurgery. Front Neurol 2020; 11:402. [PubMed: 32547470]
32. Rwigema JC, Heron DE, Ferris RL, Andrade RS, Gibson MK, Yang Y, et al. The impact of tumor volume and radiotherapy dose on outcome in previously irradiated recurrent squamous cell carcinoma of the head and neck treated with stereotactic body radiation therapy. Am J Clin Oncol 2011; 34(4):372–9. [PubMed: 20859194]
33. Tavelin B, Malmstrom A. Sex Differences in Glioblastoma-Findings from the Swedish National Quality Registry for Primary Brain Tumors between 1999–2018. J Clin Med 2022; 11(3).
34. Kim HI, Lim H, Moon A. Sex Differences in Cancer: Epidemiology, Genetics and Therapy. Biomol Ther (Seoul) 2018; 26(4):335–42. [PubMed: 29949843]
35. Massey SC, Whitmire P, Doyle TE, Ippolito JE, Mrugala MM, Hu LS, et al. Sex differences in health and disease: A review of biological sex differences relevant to cancer with a spotlight on glioma. Cancer Lett 2021; 498:178–87. [PubMed: 33130315]
36. Frosina G Radiotherapy of High-Grade Gliomas: First Half of 2021 Update with Special Reference to Radiosensitization Studies. Int J Mol Sci 2021; 22(16).
37. Shibamoto Y, Iwata H. The Quest for Optimal Fractionation Schedules in Stereotactic Radiotherapy. Cureus 2020; 12(1):e6777. [PubMed: 32117663]
38. Hingorani M, Colley WP, Dixit S, Beavis AM. Hypofractionated radiotherapy for glioblastoma: strategy for poor-risk patients or hope for the future? Br J Radiol 2012; 85(1017):e770–81. [PubMed: 22919020]
39. Lovo EE, Moreira A, Barahona KC, Ramirez J, Campos F, Tobar C, et al. Stereotactic Radiosurgery for Recurrent Glioblastoma Multiforme: A Retrospective Multi-Institutional Experience. Cureus 2021; 13(10):e18480. [PubMed: 34754642]
40. Lehrer EJ, Ruiz-Garcia H, Nehlsen AD, Sindhu KK, Estrada RS, Borst GR, et al. Preoperative Stereotactic Radiosurgery for Glioblastoma. Biology (Basel) 2022; 11(2).
41. Kim JH, Kim SH, Brown SL, Freytag SO. Selective enhancement by an antiviral agent of the radiation-induced cell killing of human glioma cells transduced with HSV-tk gene. Cancer Res 1994; 54(23):6053–6. [PubMed: 7954444]

42. Kim JH, Kim SH, Kolozsvary A, Brown SL, Kim OB, Freytag SO. Selective enhancement of radiation response of herpes simplex virus thymidine kinase transduced 9L gliosarcoma cells in vitro and in vivo by antiviral agents. Int J Radiat Oncol Biol Phys 1995; 33(4):861–8. [PubMed: 7591895]
43. Kim SH, Kim JH, Kolozsvary A, Brown SL, Freytag SO. Preferential radiosensitization of 9L glioma cells transduced with HSV-tk gene by acyclovir. J Neurooncol 1997; 33(3):189–94. [PubMed: 9195489]
44. Kim DS, Kang SK, Chi JG. Gliosarcoma: a case with unusual epithelial feature. J Korean Med Sci 1999; 14(3):345–50. [PubMed: 10402183]
45. NIH. Consideration of sex as a biological variable in NIH-funded research Notice number: NOT-OD-15–102. 2015 [Available from: https://grants.nih.gov/grants/guide/notice-files/NOT-OD-15-102.html
46. Folkman J Tumor angiogenesis: therapeutic implications. N Engl J Med 1971; 285(21):1182–6. [PubMed: 4938153]
47. Folkman J What is the evidence that tumors are angiogenesis dependent? J Natl Cancer Inst 1990; 82(1):4–6. [PubMed: 1688381]
48. Folkman J The role of angiogenesis in tumor growth. Semin Cancer Biol 1992; 3(2):65–71. [PubMed: 1378311]
49. Ewing JR, Nagaraja TN, Aryal MP, Keenan KA, Elmghirbi R, Bagher-Ebadian H, et al. Peritumoral tissue compression is predictive of exudate flux in a rat model of cerebral tumor: an MRI study in an embedded tumor. NMR Biomed 2015; 28(11):1557–69. [PubMed: 26423316]

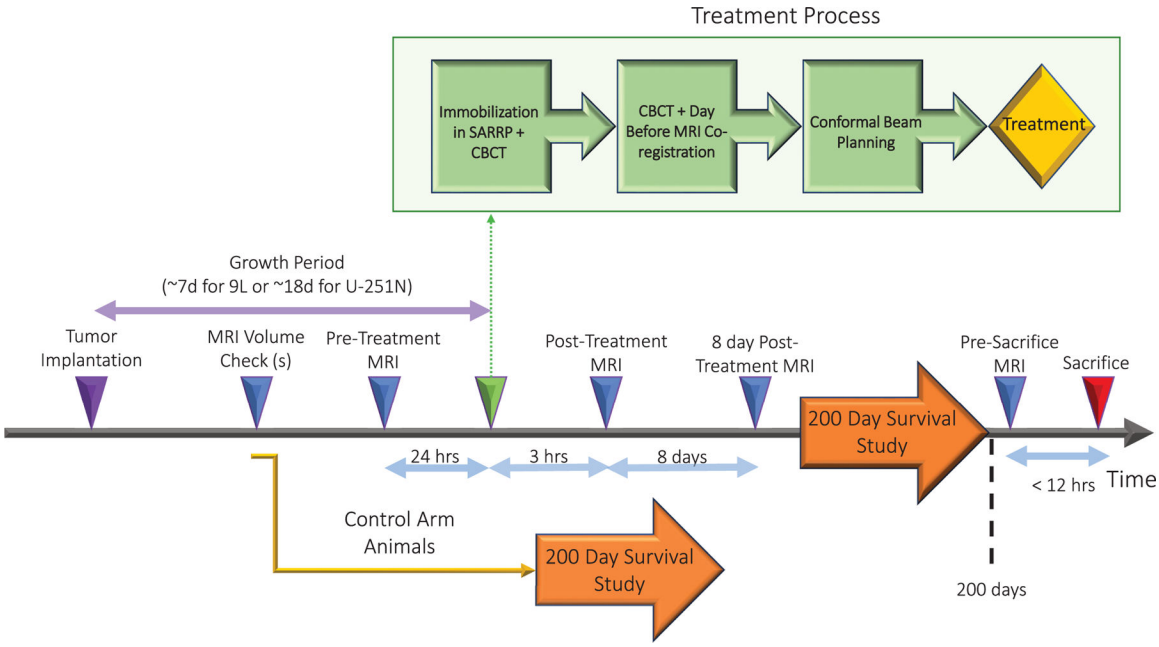

FIG. 1.

Experimental timeline from tumor implantation to death. Includes time from tumor implantation, various MRI timepoints, and a treatment breakdown.

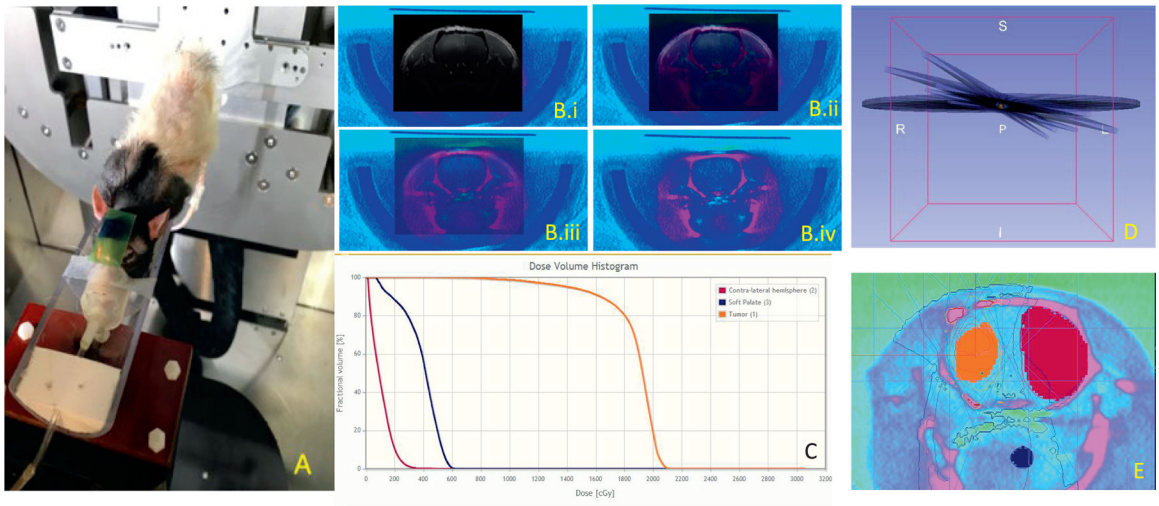

FIG. 2.

Treatment details. Panel A: The position of the rat during treatment. The image was acquired after irradiation and shows exposed GafChromic film. Panel B: An axial view of CT/3D GRE MRI co-registration with a transition from a fully opaque MRI image (panel B.i) through two intermediate steps (panels B.ii and B.iii) to a fully opaque CT image (panel B.iv). Visible soft tissue biomarkers can be seen to be in alignment throughout. Panel C: MuriPlan calculated dose volume histogram with volumes depicted in (panel E). Panel D: An example of the treatment contour with tumor (orange), contralateral hemisphere (pink), and soft palette slice (navy) with MuriPlan-calculated isodose lines. Panel E: A 3D rendering of the four non-parallel arcs used in the treatment delivery with contours of the tumor (orange), sample section of soft palate (navy), and normal, contralateral hemisphere (pink).

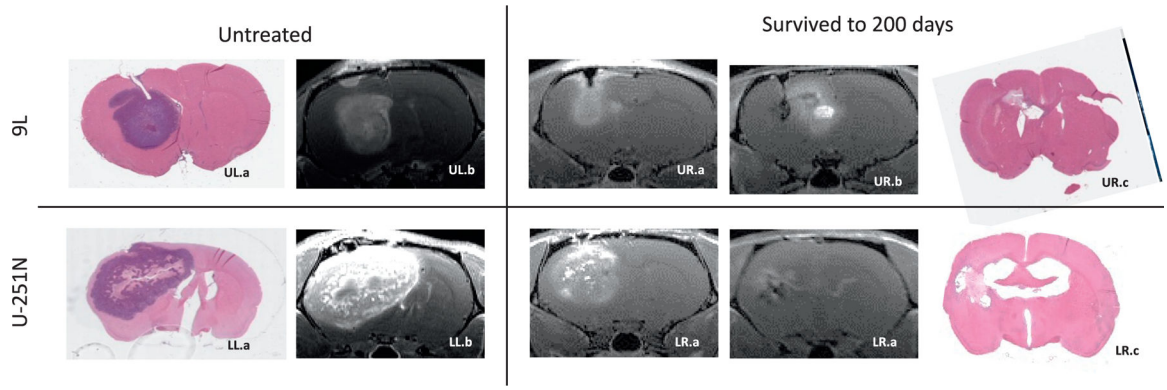

FIG. 3.

Illustration of similarity between histology and MRI in untreated controls and animals that survived to 200 days. Upper left panels: Untreated 9L (panel UL.a) hematoxylin and eosin (H&E)-stained slides and (panel UL.b) corresponding T1-weighed image estimated volume of 264 mm^3. Upper right panels: Example of a 9L tumor (panel UR.a) pre-irradiation, post-contrast T1, (panel UR.b) pre-sacrifice, post-contrast T1 and (UR.c) post-sacrifice H&E-stained section from an animal that survived to 200 days. Note the florid enhancing tumor in panel UR.a that is absent in panel UR.b. The enhancement medial to the tumor location seen in panel UR.b is partly from the enlarged 3rd ventricle below and partly due to possible radiation necrosis or pseudo progression-like development. Lower left panels: Untreated U-251N (panel LL.a) hematoxylin and eosin (H&E)-stained slides and (panel LL.b) corresponding T1-weighed image estimated volume of 2054 mm^3. H&E staining demonstrates that tumors in both tumors had well-defined boundaries. Lower right panels. Example of a U251 tumor (panel LR.a) pre-irradiation, post-contrast T1, (panel LR.b) pre-sacrifice, post-contrast T1, and (panel LR.c) post-sacrifice H&E-stained section from an animal that survived to 200 days. Note the florid enhancing tumor in panel LR.a that is absent in panel LR.b. Ventricular enlargement seen in panels LR.b and LR.c is the result of tissue loss.

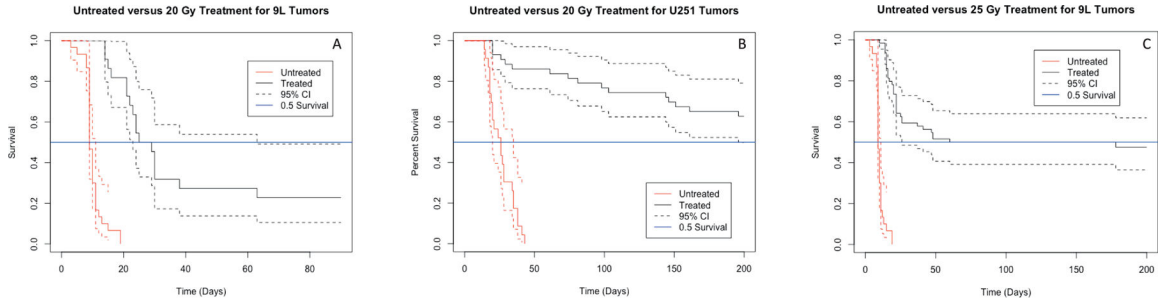

FIG. 4.

Kaplan-Meier survival curves of survival (reported in fractional survival) as a function of time for animas receiving varying radiation doses (solid lines) with 95% confidence intervals (dashed lines). Panel A: Survival of 9L-tumored control rats (n = 30, red) and those treated with 20 Gy (n = 22, black). Panel B: Survival of 9L-tumored control rats (n = 30, red) and those treated with 25 Gy (n = 64, black). Panel C: Survival of U-251N-tumored control rats (n = 23, red) and those treated with 20 Gy (n = 43, black). The time scale in panel A differs from that in panels B and C.

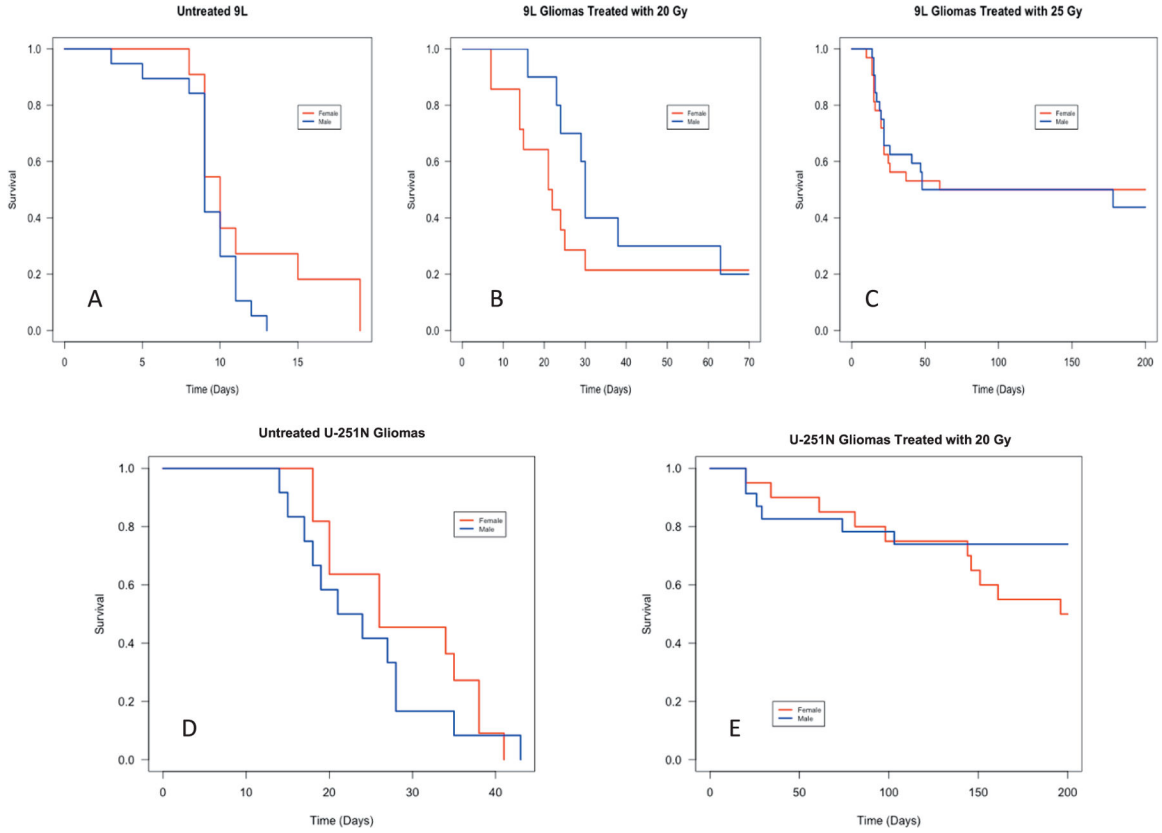

FIG. 5.

Kaplan-Meier survival curves showing a comparison of survival (reported in fractional survival) between host sex for each interest group shown in Table 1. Male survival is shown in blue, female in red. Panel A: Untreated controls with 9L tumors (m = 19, f = 11). Panel B: 9L subjects treated with 20 Gy (m = 10, f = 12). Panel C: 9L subjects treated with 25 Gy (m = 32, f = 32). Panel D: Untreated controls with U-251N tumors (m = 12, f = 11). Panel E: U-251N implanted subjects treated with 20 Gy (m = 23, f = 20). Consideration should be given to the varying time scales displayed in each figure.

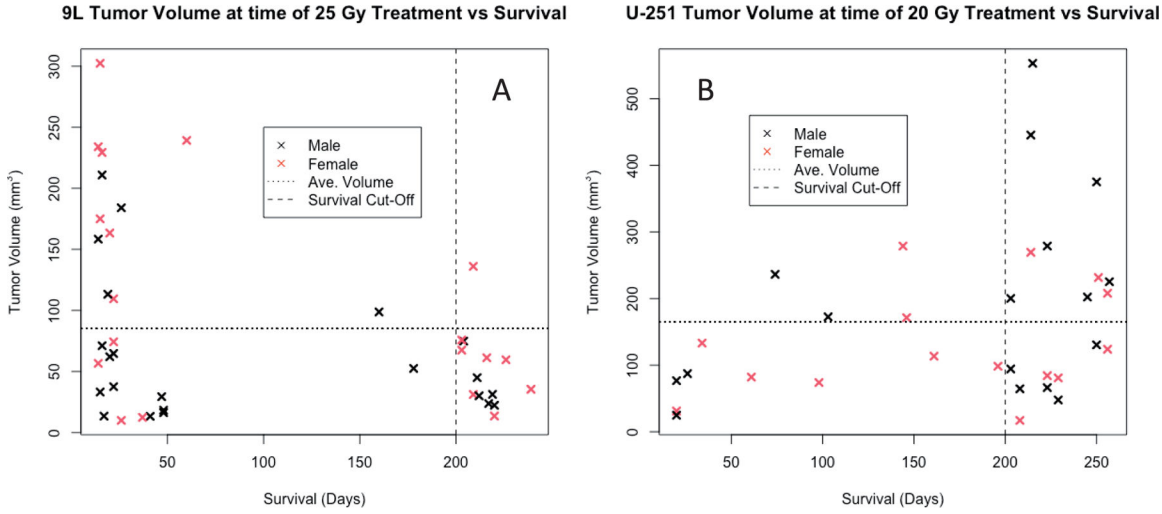

FIG. 6.

Post-contrast T1-weighted estimate of tumor volume in cubic millimeters at time of treatment versus survival in days for applicable (panel A) 9L subjects who received 25 Gy (n = 41) and panel B: U-251N subjects who received 20 Gy (n = 32). Horizontal dashed lines indicate average volumes for the groups. Vertical dashed lines indicate survival study endpoint of 200 days.

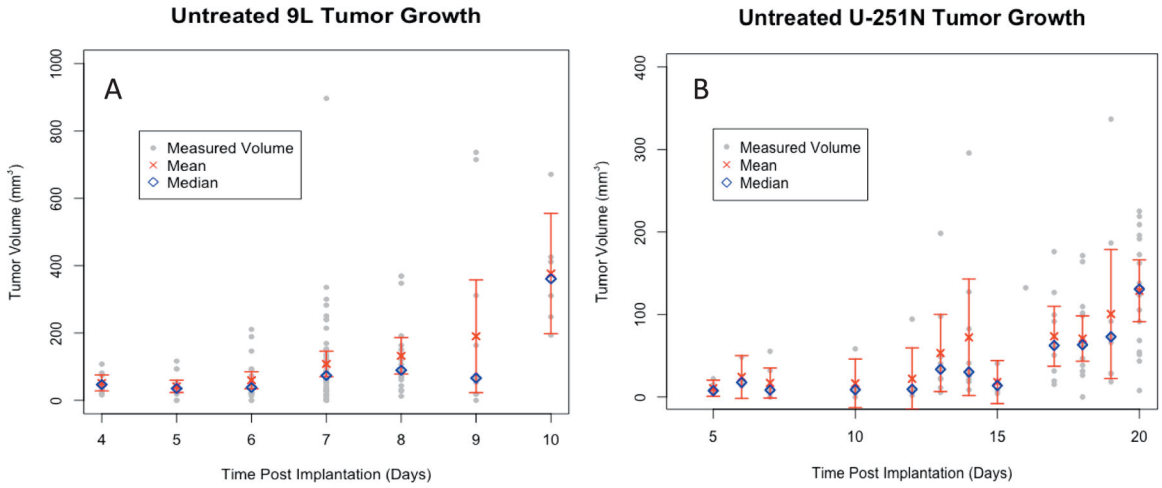

FIG. 7.

Untreated tumor growth plots. Volume from (panel A) 142 volume measurements in mm^3 of untreated 9L tumors from 105 animals and (panel B) 142 volume measurements in mm^3 of untreated U-251N tumors from 80 animals plotted against days post-implantation. Measured volumes are shown in gray alongside the mean (red ×), median (blue diamond), and 95% CI error bars of the mean for each day.

*Additional untreated tumors from different radiation treatment protocols not presented in this paper were included in this data set.

TABLE 1

Number of Animals Utilized in Survival Studies Broken Down by Sex, Treatment and Species

Animal Type	Fischer 344 Rat with 9L Tumors		Totals	RNU Athymic Rat with U-251N Tumors		Totals
Sex	Male	Female	-	Male	Female	-
Control	19	11	30	12	11	23
Treated with 20 Gy	10	12	22	23	20	43
Treated with 25 Gy	32	32	64	0	0	0
Total	61	55	116	35	31	66
Total Included in Study	116			66		

TABLE 2

Kaplan-Meier Analysis

Tumor group	Treatment dose	n	Events	Median survival (95% CI) [days]	Restricted mean** survival ± standard error (days)
9L	Untreated control	30	30	9 [9,11]	10 ± 1
	20 Gy	22	17	27 [23,63]	65 ± 16
	25 Gy	64	33	119 [26, >200]	111 ± 11
U-251N	Untreated control	23	23	26 [20,35]	26 ± 1
	20 Gy	43	16	> 200 [196, >200]	157 ± 10

Notes. Survival is stated as median survival time for “n” animals in days based on events of death or COVID censorship, with 95% confidence limits in brackets and restricted mean survival in days plus or minus its standard error.

** Restricted with an upper limit of survival of 200 days.

TABLE 3

Cox Proportional Hazards (PH) Model Analyses Comparing Survival for each Interest Group in Terms of Animals' Sex

Sex effect on survival (Cox-PH model)				
Tumor group	**Treatment dose**	**n (M/F)**	**HR (M/F) [95% CI]**	**P value**
9L	Untreated control	30 (19/11)	1.88 [0.81, 4.34]	0.141
	20 Gy	22 (10/12)	0.72 [0.28,1.88]	0.506
	25 Gy	64 (32/32)	1.06 [0.51,2.01]	0.965
U-251N	Untreated control	23 (12/11)	1.35 [0.58,3.15]	0.486
	20 Gy	43 (23/20)	0.51 [0.19,1.42]	0.199

Notes. Results are reported as hazard ratio (HR) with 95% confidence limits in brackets. The P value is used to reject the null hypothesis that HR = 1, i.e., a P value < 0.05 suggests that there is a gender effect on survival.

TABLE 4

Summary of Statistics Pertaining to the Tumor Volume at Time of Treatment for U-251N Tumors Treated with 20 Gy and 9L Tumors Treated with 25 Gy

Summary of available volume at time of treatment data				
Group	**n**	**Mean volume ± standard error (mm_3)**	**Volume range [min, max] (mm^3)**	**Volume median (mm^3)**
U-251N 20 Gy	32	165.0 ± 22.0	[17.1, 553.2]	127.2
U-251N 20 Gy survivors	19	194.7 ± 32.9	[17.1, 553.2]	200.3
U-251N 20 Gy non-survivors	13	121.5 ± 21.0	[24.8, 278.8]	98.4
9L 25 Gy	41	85.2 ± 11.9	[10.0, 302.4]	61.3
9L 25 Gy survivors	14	50.6 ± 8.6	[13.6, 136.1]	40.2
9L 25 Gy non-survivors	27	103.1 ± 16.6	[10.0, 302.4]	71.1

Note. Data is presented in Table 5 and Fig. 6.

TABLE 5

Wilcoxon Rank Sum Test to Assess the Effect of Measured Tumor Volume at Time of Treatment on Survival as a Binary Outcome (Yes, Survival to 200 Days or No, Died before 200 Days) for Tumors Treated with a ~50% Curative Dose

Results of Wilcoxon Rank Sum Te			
Group	**n**	**W value**	**P value**
U-251N 20 Gy	32	156	0.223
U-251N 20 Gy males	17	41	0.279
U-251N 20 Gy females	15	31	0.779
9L 25 Gy	41	137	0.159
9L 25 Gy males	22	36	0.407
9L 25 Gy females	19	24	0.109

Notes. The W-test statistic is reported for each group and represents the minimum rank available for each group evaluated. P values are presented at the 95% CI and evaluate the null hypothesis that the population of survivors and non-survivors are the same based on treated tumor volume, i.e., a P value < 0.05 suggests that the two populations deviate.